DOI: 10.1002/ejic.200801084

Solvothermal Syntheses of Two New Thiostannates and an In-Situ Energy Dispersive X-ray Scattering Study of Their Formation

Nicole Pienack,[a] Christian Näther,[a] and Wolfgang Bensch*[a]

Keywords: Solvothermal synthesis / Energy-dispersive X-ray diffraction / Thiostannates / Mixed-valent compounds / Kinetics / Reaction mechanisms

Two new thiostannates, $(DBNH)_2Sn_3S_6$ (**1**) and $(DBNH)_2Cu_6Sn_2S_8$ (**2**), were synthesized under solvothermal conditions using Cu, Sn, S and DBN (DBN = 1,5-diazabicyclo[4.3.0]non-7-ene). Compound **1** is a rare example of a mixed-valent thiostannate. The Sn^{II} center exists in the rare trigonal pyramidal coordination environment, whereas Sn^{IV} is tetrahedrally coordinated. The chain-anion is composed of alternating Sn_3S_4 semi-cubes and Sn_2S_2 rings. The structure of **2** consists of undulated anionic layers with amine molecules between the layers. The layers may be viewed as a heteroatom 6^3 graphene layer constructed of condensed CuS_3 triangles and SnS_4 tetrahedra. The two thiostannates coexist, and this was investigated with in-situ energy dispersive X-ray scattering under solvothermal conditions. Prior to the formation of **1** and **2**, a crystalline intermediate appears, which disappears after 60 min. Then reflections of **2** start to grow, and reflections of **1** appear some time later. The appearance of a thiostannate(IV) species followed by the crystallization of a mixed-valent thiostannate(II,IV) species suggests that complex redox reactions are occurring under the solvothermal conditions. Syntheses without Cu in the reaction slurry lead to the formation of **1** within a very short time period. The results of the in-situ studies clearly indicate that the presence of Cu species in solution retards the nucleation and crystallization of **1**. The crystalline intermediate was quenched with ex-situ experiments. All syntheses performed with this intermediate do not lead to the crystallization of **1** or **2**, i.e., there is no direct relation between these three crystalline compounds. The spectroscopic and thermal properties of **1** and **2** are also discussed.

Introduction

Several thiostannates have been synthesized through a solvothermal route using different amines as structure directing agents such as $^1_\infty[SnS_2{\cdot}en]$ (en = ethylenediamine),[1] $(C_6H_{20}N_4)_2[Sn_2S_6]{\cdot}2H_2O$,[2] $(C_2H_{10}N_2)(C_2H_9N_2)_2[Sn_2S_6]$,[3] $R_2Sn_3S_7$ [R = tetramethylammonium (TMA),[4] diazabicyclooctane (DABCO),[5] ammonium/tetraethylammonium (ATEA), tetraethylammonium (TEA)[6]], $R'_2Sn_4S_9$ [R′ = tetrapropylammonium (TPA), tetrabutylammonium (TBA)[6]] and $(enH)_4[Sn_2S_6]$.[7] Besides having interesting structural features, thiostannates are candidates for catalysis applications and chemical sensing.[8–10] In addition, the integration of transition metals (TMs) into their crystalline networks alters their physical and chemical properties.[11] Some examples of thiostannates containing transition metals are $[Ni(en)_3]_2Sn_2S_6$, $[Co(tren)]_2Sn_2S_6$ [tren = tris(2-aminoethyl)-amine], $[Ni(tren)]_2Sn_2S_6$,[12] $(1,4\text{-dabH}_2)Ag_2SnS_4$ (1,4-dab = 1,4-diaminobutane),[13] (DBUH)$CuSnS_3$ (DBU = 1,5-diazabicyclo[4.3.0]non-5-ene), $(1,4\text{-dabH}_2)Cu_2SnS_4$,[14] $[Ni(dien)_3]_2Sn_2S_6$ (dien = diethylenetriamine)[15] or $[M(en)_3]_2Sn_2S_6$ (M = Mn, Co, Zn).[16] Sn^{IV} is the most common oxidation state in thiostannates and tin sulfides. Until now the number of mixed-valent Sn sulfides has been limited, with the most famous example of these being Sn_2S_3, which contains Sn^{II} and Sn^{IV}.[17] However, there are some other compounds like $K_2Sn_4Se_8$,[18] $Rb_2Sn_4Se_8$, $Cs_2Sn_4Se_8$,[19] $[Sn_2I_3(NPPh_3)_3]$,[20] $[Sn(\mu_3\text{-}NSnMe_3)]_4$,[21] $In_2Sn_3S_7$,[22] $In_6Sn_8S_{19}$,[23] $Sn_5Sb_2S_9$[24] and $Cr_2Sn_3Se_7$,[25] which feature the coexistence of Sn^{II} and Sn^{IV} oxidation states.

A well-known problem in solvothermal syntheses is that in these heterogeneous multicomponent processes many parameters such as temperature, time, solvent and concentration influence the product formation. Despite several efforts undertaken by different groups, we are far from achieving a deeper understanding of the reaction mechanisms occurring under solvothermal conditions.[26] The following example should illustrate the main problems of the solvothermal approach: syntheses performed with Sb, S, Ni and diethylenetriamine as structure directing agent lead to a number of compounds such as $[Ni(dien)_2]_2Sb_4S_8$,[27] $[Ni(dien)_2]_2Sb_4S_9$[28] or $[Ni(dien)_2]_3(Sb_3S_6)_2$[29] under almost identical conditions.

In order to shed light on some aspects of the phenomena occurring under solvothermal conditions and to get more information about such 'black-box reactions', kinetic analyses applying in-situ methods are necessary. During the last few years we successfully investigated several solvothermal

[a] University of Kiel, Institute of Inorganic Chemistry, Max-Eyth-Str. 2, 24118 Kiel, Germany
Fax: +49-4318801520
E-mail: wbensch@ac.uni-kiel.de

reactions by applying time-resolved in-situ energy-dispersive X-ray diffraction (in-situ EDXRD).[30–36] This technique facilitates investigations of the influence of different parameters on product formation under real reaction conditions.[10,37] The appearance, growth and decay of crystalline precursors or intermediates can be directly observed, which is not possible with ex-situ experiments. In addition, it is possible to determine directly whether such transient compounds are related to or necessary for the crystallization of the product. Finally, these studies supply the necessary reaction conditions for quenching such precursors and/or intermediates. In our ongoing work in the field of the solvothermal syntheses of transition-metal-containing thiostannates, we studied solvothermal reactions using Cu, Sn, S and 1,5-diazabicyclo[4.3.0]non-5-ene (DBN) as solvent and structure directing agent. An interesting result observed during the solvothermal syntheses is the coexistence of two thiostannates, one of which is a Sn^{II}/Sn^{IV} mixed-valent compound without Cu and a second which contains Cu and Sn^{IV}. This experimental finding requires a systematic study of the solvothermal reaction, and investigations using in-situ EDXRD were appropriate for this purpose. In this paper we present the solvothermal syntheses of two new thiostannates, $(DBNH)_2Sn_3S_6$ (**1**) and $(DBNH)_2Cu_6Sn_2S_8$ (**2**), their crystal structures, their thermal and spectroscopic properties and the results of the in-situ EDXRD studies.

Results and Discussion

The new $(DBNH)_2Sn_3S_6$ thiostannate (**1**) crystallizes in the monoclinic space group $P2_1/n$ space group with all atoms located on general positions. The three unique Sn atoms are in different coordination environments. Sn(1) and Sn(2) are surrounded by five S atoms forming distorted rectangular pyramids (Figure 1). The Sn–S bonds range from 2.3901(14) to 2.7024(13) Å for Sn(1) and from 2.3937(14) to 2.7157(13) Å for Sn(2) (Table 1), with corresponding S–Sn–S angles varying from 86.64(4) to 126.39(6)°.

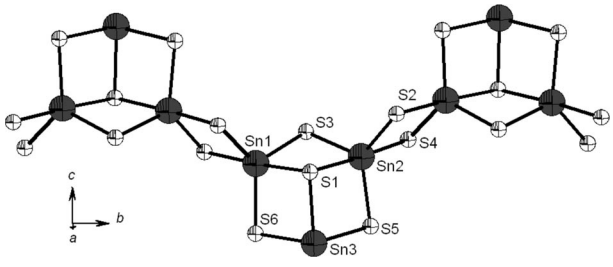

Figure 1. The anionic chain directed along [010] together with atom labelling. The displacement ellipsoids are drawn at the 50% probability level.

These values are in good agreement with literature data.[38,39] Interestingly, Sn(3) is surrounded by only three S atoms to form a trigonal pyramidal SnS_3 unit. This geometry is an indication for a Sn^{II} oxidation state, and bond valence calculations confirm both this assignment as well as the mixed-valent character of $(DBNH)_2Sn_3S_6$ (all parameters for the calculations were taken from ref.[40]). The Sn–S bond lengths in the SnS_3 pyramid are 2.5059(13), 2.5335(16) and 2.5511(17) Å (average Sn–S distance: 2.5302 Å), with the corresponding angles being 88.02(4), 88.62(4) and 102.39(6)°. The existence of Sn in a trigonal pyramidal environment is quite rare, but some examples of compounds in which this occurs are Ottemannite $[Sn(SnS_3)]$,[41] $C_{25}H_{27}NO_3SnS_3$,[42] $C_{42}H_{35}AsSnS_3$,[43] and $C_{42}H_{35}PSnS_3$.[44] In these compounds the Sn–S bond lengths range from 2.532(10) to 2.765(2) Å, and the S–Sn–S angles scatter from 83.59(2) to 96.87(3)°. The two SnS_5 pyramids and the SnS_3 group share common edges to form a so-called Sn_3S_4 semi-cube (Figure 1). Neighboring semi-cubes are joined through the terminal S atoms of the SnS_5 groups to yield a one-dimensional anionic $[Sn_3S_6]^{2-}$ chain running along the [010] direction (Figure 1). Alternatively, the structure of the chain may be viewed as alternating Sn_3S_4 semi-cubes and Sn_2S_2 rings.

Table 1. Bond lengths [Å] for **1**.

Sn(1)–S(4)	2.3901(14)
Sn(1)–S(6)	2.3927(14)
Sn(1)–S(3)	2.4149(12)
Sn(1)–S(2)	2.5367(14)
Sn(1)–S(1)	2.7024(13)
Sn(2)–S(5)	2.3937(14)
Sn(2)–S(2)[a]	2.4020(13)
Sn(2)–S(3)	2.4201(12)
Sn(2)–S(4)[a]	2.5222(14)
Sn(2)–S(1)	2.7157(13)
Sn(3)–S(1)	2.5059(13)
Sn(3)–S(5)	2.5335(16)
Sn(3)–S(6)	2.5511(17)

Symmetry transformations used to generate equivalent atoms:
[a] $-x + 3/2, y + 1/2, -z + 1/2$

Within the chains, the Sn_3S_4 semi-cubes are arranged in a zigzag-like fashion, and the amine molecules are located in the cavities of neighboring chains (Figure 2). In contrast with other compounds containing Sn_3S_4 units, the divalent Sn atom of the Sn_3S_4 semi-cube in **1** is trigonally coordinated and has no contact to other sulfur atoms (see Figure 1). Short S···H–N separations [S(1)–N(2): 3.388(17) Å and S(2)–N(4): 3.499(2) Å] indicate weak hydrogen bonding interactions.

An interesting observation is that the anionic chain of $(DBNH)_2Sn_3S_6$ shows structural motifs similar to those in the layered R–SnS-1 and R–SnS-3 (R = organic molecule) thiostannates.[38,39] In these compounds, two-dimensional $[Sn_3S_7]^{2-}$ and $[Sn_4S_9]^{2-}$ anionic layers are also observed to contain Sn_3S_4 semi-cubes, which are formed by the interconnection of SnS_5 trigonal bipyramids. The semi-cubes are joined through two S^{2-} anions to yield anionic layers with rings consisting of 24 atoms (largest interatomic distance: 10 Å). The organic molecules act as charge-compensating cations and are located above/below the pores and between the layers.[45] In R–SnS-3 thiostannates, the Sn_3S_4 units are joined by SnS_4 tetrahedra to form $[Sn_4S_9]^{2-}$ layers with elliptical rings measuring about 19.8×11.3 Å in diameter for

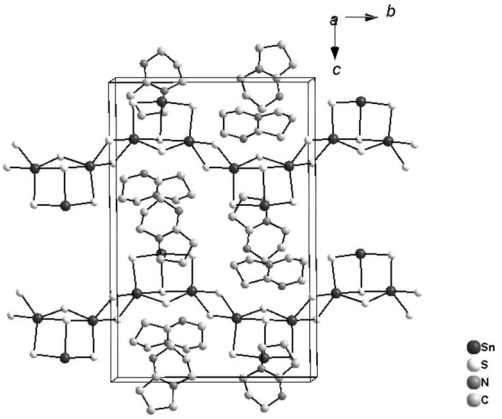

Figure 2. Packing in the *bc* plane of $(DBNH)_2Sn_3S_6$ with undulated chains along the [010] direction. H atoms are omitted for clarity.

TBA–SnS-3 (TBA = tetrabutylammonium).[6] Alkali metal ions were used instead of organic structure directing agents for the synthesis of thiostannates like $Rb_2Sn_3S_7{\cdot}2H_2O$ or $Cs_4Sn_5S_{12}{\cdot}2H_2O$,[46,47] which also contain Sn_3S_4 groups as well as Sn_2S_2 rings. In $Cs_4Sn_5S_{12}{\cdot}2H_2O$, two Sn_3S_4 semi-cubes are connected via a common corner through two bridging S^{2-} anions to form the anionic layers containing elliptical pores of about 7.3×9.9 Å in diameter. In $Rb_2Sn_3S_7{\cdot}2H_2O$, the anionic layers are constructed of face-sharing semi-cubes and bridging Sn_2S_2 rings.

The second new compound, $(DBNH)_2Cu_6Sn_2S_8$ (**2**), crystallizes in the noncentrosymmetric orthorhombic space group $Pca2_1$ space group with two unique Sn, six Cu and eight S atoms, as well as two protonated DBN molecules. All atoms are located on general positions. The structure consists of undulated anionic layers in the (1 0 0) plane and protonated amine molecules acting as charge-compensating cations between the layers (Figure 3).

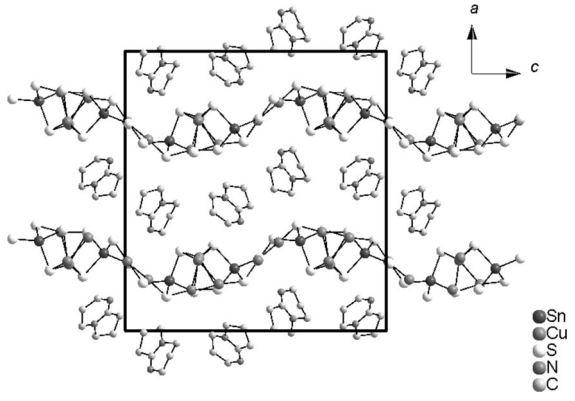

Figure 3. Arrangement of the undulated anionic layers and the cations in compound **2** (viewed along the *b* axis). H atoms are omitted for clarity. Some DBN molecules are disordered and the split positions are not displayed.

Each Sn atom is tetrahedrally coordinated by S atoms, with Sn–S distances ranging from 2.392(2) to 2.414(2) Å (Table 2) and S–Sn–S angles ranging from 109.98(9) to 112.90(8)°, which indicates a moderate deviation from ideal tetrahedral geometry. These values match well with data published in the literature.[12,48]

Table 2. Bond lengths [Å] for **2**.

Sn(1)–S(2)[a]	2.392(2)	Cu(3)–S(4)	2.238(2)
Sn(1)–S(3)	2.405(2)	Cu(3)–S(8)	2.357(3)
Sn(1)–S(6)	2.407(2)	Cu(3)–S(5)	2.446(3)
Sn(1)–S(4)	2.414(2)	Cu(3)–Cu(4)	2.7755(18)
Sn(1)–Cu(6)	3.1678(18)	Cu(3)–Cu(5)	3.052(2)
Sn(2)–S(1)[b]	2.385(2)	Cu(4)–S(6)[a]	2.240(2)
Sn(2)–S(8)	2.408(2)	Cu(4)–S(2)[a]	2.246(2)
Sn(2)–S(5)	2.427(2)	Cu(4)–S(5)	2.295(2)
Sn(2)–Cu(3)	3.0951(13)	Cu(5)–S(7)	2.241(2)
		Cu(5)–S(5)	2.268(2)
Cu(1)–S(1)	2.239(2)	Cu(5)–S(6)	2.284(2)
Cu(1)–S(7)[c]	2.249(2)	Cu(5)–Cu(6)	2.833(2)
Cu(1)–S(3)	2.282(2)	Cu(6)–S(8)[d]	2.200(3)
Cu(2)–S(2)	2.220(3)	Cu(6)–S(4)	2.260(3)
Cu(2)–S(1)[d]	2.258(3)	S(1)–Cu(2)[a]	2.258(2)
Cu(2)–S(3)	2.277(2)	S(1)–Sn(2)	2.385(2)

Symmetry transformations used to generate equivalent atoms: [a] $x, y + 1, z$. [b] $-x + 3/2, y, z - 1/2$. [c] $-x + 3/2, y, z + 1/2$. [d] $x, y - 1, z$

All of the Cu atoms are bound to three S atoms to form distorted CuS_3 triangles, with the Cu atoms being located slightly above the planes formed by the three S atoms. The Cu–S bond lengths scatter between 2.200(3) and 2.446(3) Å (Table 2), and the corresponding angles range from 97.88(8) to 141.84(15)°. All of these values are in the typical range reported in the literature.[14,49,50] The Cu(3) to Cu(6) atoms each have another Cu atom within a distance ranging from 2.7755(18) to 3.052(2) Å (Table 2). Some examples of compounds with comparable values for such Cu–Cu distances are $(enH_2)_{0.5}Cu_2SbS_3$ (en = ethylenediamine), $(1,3\text{-}dapH_2)_{0.5}Cu_2SbS_3$ (1,3-dap = 1,3-diaminopropane),[51] $(C_6N_4H_{20})_{0.5}Cu_3Sb_2S_5$[52] and $(1,4\text{-}dabH_2)Cu_2SnS_4$ (1,4-dab = 1,4-diaminobutane).[14] In the literature, d^{10}–d^{10} interactions are discussed for several sulfides,[53] but in those cases the Cu–Cu distances are even shorter than in compound **2**.

CuS_3 triangles and SnS_4 tetrahedra are joined to form six different six-membered Cu_2SnS_3 heterorings: Cu(4)-Cu(5)Sn(1)S_3 (A), Cu(1)Cu(5)Sn(2)S_3 (B), Cu(1)Cu(2)-Sn(1)S_3 (C), Cu(2)Cu(4)Sn(2)S_3 (D), Cu(4)Cu(5)Sn(2)S_3 (E) and Cu(1)Cu(2)Sn(2)S_3 (F), which are condensed in the (1 0 0) plane (Figure 4, left) to yield an undulated layer which may be viewed as a distorted graphene 6^3 layer.

Along the [001] direction, the sequence of the rings is ...A–B–C–... and ...D–E–F... The Cu(3)S_3 and Cu(6)S_3 units do not participate in these rings; they are instead joined into chains along the [010] direction by corner-sharing with each other and edge-sharing with the SnS_4 tetrahedra (Figure 4, right). The chains and layers are connected through the S atoms of the SnS_4 tetrahedra. This connection scheme leads to the formation of further heterorings like Cu(3)-Cu(4)Cu(5)S_3 and Cu(4)Cu(6)Sn(2)S_3. The structural motif of condensed six-membered rings is found in layered thioantimonates like $(C_4N_3H_{14})Cu_3Sb_2S_5$ and $(C_6N_4H_{20})_{0.5}Cu_3Sb_2S_5$,[49] but has not been observed before in thiostannates. The amine molecules are located between the layers with an interlayer distance of about 7.5 Å. Short S···H–N separations [S(3)–N(4): 3.162(14) Å and S(3)–N(2): 3.313(27) Å] indicate weak hydrogen bonding interactions.

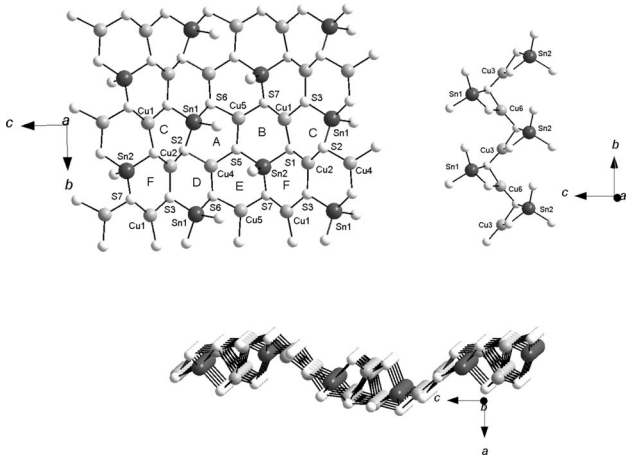

Figure 4. Condensation of the different heterorings in compound **2** forming the anionic layer (top, left). The chain made up by interconnection of $Cu(3)S_3$, $Cu(6)S_3$ and SnS_4 tetrahedra (top, right). Undulated arrangement of a layer (as viewed approximately along the *b* axis) (bottom).

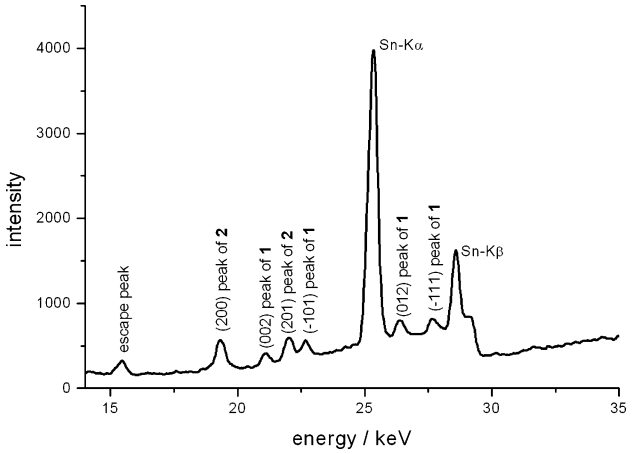

Figure 5. A typical powder pattern recorded at the F3 beamline. The Bragg reflections of both compounds and the Sn fluorescence peaks are labelled. The peak at ca. 15.5 keV is the escape peak of the Ge detector.

In-Situ EDXRD Investigations

Solvothermal syntheses are often complicated by the products not being of a pure phase, and sometimes even in one reaction mixture thiometalates with different compositions coexist. This problem is exemplified in the synthesis of $[Ni(dien)_2]Sb_4S_7{\cdot}H_2O$ where the product always contains $[Ni(dien)_2]_3(SbS_4)_2$[54] as a second phase. In the present case, not only do two different thiostannates coexist, but these two compounds have Sn centers in different oxidation states. Elemental Sn and Cu are used in the syntheses, and obviously complex redox reactions lead to the formation of Sn^{II} and Sn^{IV} in **1** and Sn^{IV} in **2**. The synthesis was performed under a broad range of conditions to increase the yields and to find conditions where only compound **2** appears in the final product. However, after about 50 syntheses without success, the question of whether the occurrence of the two products is an inherent "problem" was raised. Several scenarios can be imagined: (i) both compounds crystallize simultaneously and coexist as they possess similar stabilities; (ii) one of the two compounds is formed first, and the second starts to form at later stages of the reaction; for instance, the Cu-containing material (**2**) appears first and is partially dissolved to provide the species necessary for the crystallization of **1**.

The energy range of the spectra was chosen to show at least two reflections of the final products of both compounds at the same time. A typical spectrum obtained at the end of a reaction with Cu, Sn, S and DBN shows the Sn-*Kα* and Sn-*Kβ* fluorescence peaks as well as the Bragg peaks of the two compounds (Figure 5).

The progress of a typical reaction at 160 °C is shown as time-resolved spectra in Figure 6. In the beginning of the reaction, only Sn fluorescence peaks are observable, and a crystalline intermediate starts to appear (marked in Figure 6) after about 8 min. This intermediate survives approximately 60 min, and when this phase has disappeared, the (200) and (201) reflections of **2** become visible after 68 min and 72 min, respectively. After a reaction time of 110 min, the Cu-free compound **1** starts to appear with all reflections growing at the same reaction time.

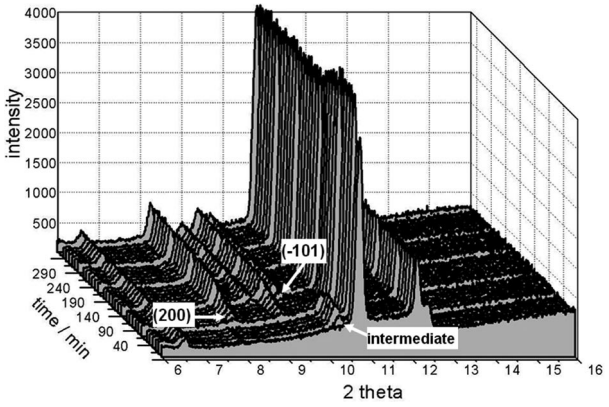

Figure 6. Time-resolved powder diffraction patterns of a synthesis at 160 °C. The reflection of the crystalline intermediate, the (–101) reflection of $(DBNH)_2Sn_3S_6$ (**1**) and the (200) reflection of $(DBNH)_2Cu_6Sn_2S_8$ (**2**) are marked. The energy is converted into the 2θ scale by applying the Cu-K_α wavelength. The peak at ca. 6.6° 2θ is the escape peak of the Ge detector.

First we analyze the crystallization kinetics of compound **2**. The evaluation of the data for **1** is difficult because of the relatively low intensity of the reflections belonging to this compound and their overlap with the reflections of **2**. In principle a deconvolution of superimposed reflections is possible with the program calf3 (see experimental section), and this analysis was also done. However, the scattering of the intensity of the two reflections was too large for an unambiguous analysis of the crystallization kinetics. In the literature, different models for the crystallization kinetics and the evaluation of appropriate data are well documented.[55–59] In the majority of cases kinetics are evaluated using Johnson–Mehl–Avrami (JMA) kinetics. Several strict

conditions such as random nucleation and no hard impingement have to be fulfilled before the JMA kinetics will hold. The JMA kinetics do not take into account that different reactions can occur in a parallel and/or successive fashion. In addition, it is assumed that the reaction exponent m is temperature and time independent, which is not necessarily the case. Therefore, the experimentally derived reaction exponents often differ from the theoretical values.

The kinetic analyses are done by integrating the intensities of the product reflections, which are normalized against the intensities of the Sn-*Ka* fluorescence peaks. The experimental data are expressed as the extent of reaction and compared with the theoretical values for solid-state kinetics. $\alpha(t)$ is the ratio of the normalized intensity at time t to the intensity at time t_∞ and is defined by the following equation:

$$\alpha(t) = I_n(t)/I_n(t_\infty)$$

Using the Avrami-Erofeev expression, the kinetic parameters for the reaction exponent m (Avrami exponent) and the rate constant k can be estimated. The kinetic parameters can also be extracted using a Sharp–Hancock (SH) plot.[56] The reaction exponent m corresponds to the slope of the curve, and the rate constant k is the intercept with the y axis. If the reaction follows one mechanism over the whole reaction time, all experimental data points are on a straight line in a SH plot. Therefore, a change in mechanism during a reaction can be detected immediately. For the evaluation of the kinetic data, the induction time t_0 was subtracted from the time t. The SH plot for the (200) peak of **2** at 160 °C is shown in Figure 7.

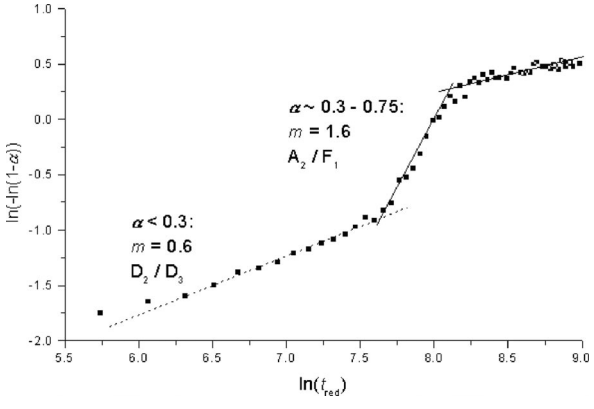

Figure 7. Sharp–Hancock plot for the reaction at 160 °C using the (200) reflection of **2**. The lines are guides for the eyes.

The growth of **2** can be roughly divided into three different parts. Up to $\alpha(t) \approx 0.3$, the value for m is about 0.6, which is near models for diffusion control (D_2/D_3). In the second part ($0.3 < \alpha < 0.75$), m increases to 1.6, which indicates a change in mechanism. This value is in between the nucleation Avrami model A_2 and a first-order reaction (F_1). For $\alpha > 0.75$, m decreases to about 0.4. In the present case it seems that no simple kinetic behavior dominates the reaction. This is further evidenced by plotting $t/t_{0.5}$ vs. α to allow a direct comparison with the established models (Figure 8).

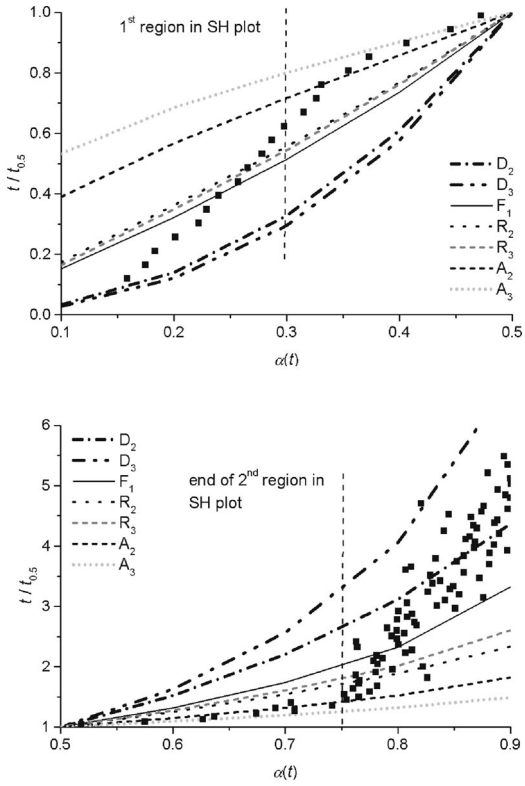

Figure 8. Comparison of different kinetic models at 160 °C using the data for the (200) peak.

In the region between $\alpha(t) = 0.1$ and 0.5 (Figure 8, top), the experimental data points gradually shift from diffusion control to Avrami nucleation models (A_2/A_3) with increasing reaction time. In Figure 8 (bottom) the data points between $\alpha(t) = 0.4$ and 0.75 suggest that Avrami nucleation models dominate the kinetics. For the later stages of the reaction, the data points scatter with a tendency toward a diffusion control model. Two different cases can be distinguished for Avrami nucleation: (i) all nuclei form instantaneously (zero order) or (ii) nuclei are added as the reaction progresses (first order).

The reaction exponent m contains information on the morphology and kinetics, and taking into account the two-dimensional nature of the crystals, $m \approx 1.6$ implies a two-dimensional growth and instantaneous formation of the nuclei. The deviation of m from the ideal value of 2 may be caused by heterogeneous nucleation on the walls of the glass tube. For all temperatures a change of m is observed over the course of the reaction, with a tendency for this change to occur at later stages of the reaction. The reactions performed without Cu are very fast, and all reflections appear simultaneously after short induction times (Figure 9). In this case, a quantitative evaluation of the reaction kinetics is not possible because of the fast reaction progress.

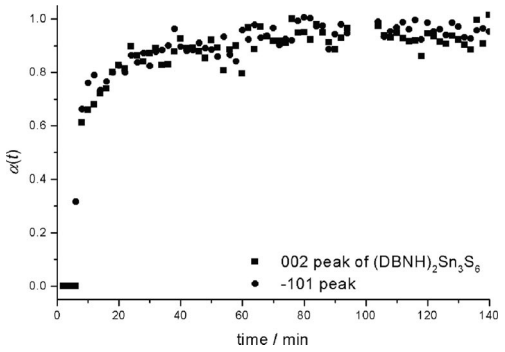

Figure 9. Extent of reaction for compound **1** at 170 °C synthesized without Cu in the reaction mixture.

As mentioned above, prior to the formation of **1** and **2** a crystalline intermediate appears during the syntheses with Cu, Sn, S and DBN. In syntheses performed without Cu, no crystalline precursor or intermediate could be observed in the temperature window from 140 to 190 °C. This is a clear indication that the crystalline intermediate species occurs only in the presence of Cu in the reaction slurry. In addition, the presence of Cu is not required for the crystallization of the mixed-valent compound **1**, i.e., Cu is not involved in the redox reaction. For the chemical characterization of the crystalline intermediate, this phase was isolated by quenching the reaction at different reaction times. For the intermediate quenched after 30, 40, 50 and 60 min, EDX analyses give nearly identical ratios for Cu/Sn/S of about 2:1:6. The CHN content is in agreement with there being about one DBN molecule in the formula if Cu_2SnS_6 is assumed to be the chemical composition of the inorganic part; i.e., the chemical formula of the intermediate is most likely $(DBNH_2)Cu_2SnS_6$. Charge neutrality of this compound requires the presence of S_2^{2-} anions if the presence of Cu^{I}, Sn^{IV} and a doubly protonated DBN molecule are assumed.

More information about the role of the intermediate species in the formation of **1** and **2** can be extracted by comparing the evolution of the extent of reaction for the intermediate phase and compounds **1** and **2** (Figure 10). Obviously, compound **2** starts to appear after the intermediate disappears. The crossing point of the $\alpha(t)$ value of the intermediate with that of **2** is far below α = 0.2–0.3, and may even be at α = 0. A possible interpretation for this observation is that the intermediate is a metastable compound which is destroyed before the more stable compounds start to form. Furthermore, the first reflections of **1** appear when roughly 40% of compound **2** is formed. At longer reaction times both compounds are in equilibrium, which supports the observation of the ex-situ syntheses presented above. Within experimental accuracy, no decrease in the intensity of the reflections of **2** is observed, which indicates that **1** does not form at the expense of **2**. We note that only at T = 160 and 170 °C does the crystalline intermediate appear. At higher temperatures no reflections of this intermediate are detected. Two possibilities can be envisaged to explain this observation: (i) the crystalline transient compound is not formed at higher temperatures or (ii) the experimental time scale is too slow for the detection of this compound because of its very fast formation and disappearance.

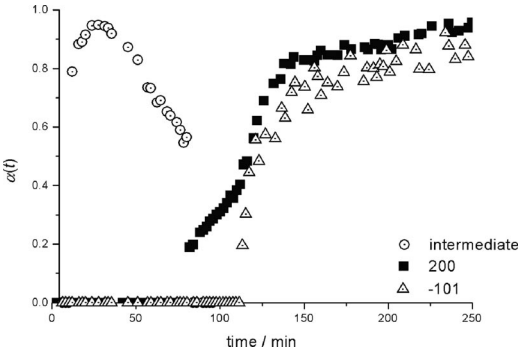

Figure 10. The extent of reaction $\alpha(t)$ for the (200) reflection of $(DBNH)_2Cu_6Sn_2S_8$ (**2**), the (–101) reflection of $(DBNH)_2Sn_3S_6$ (**1**) and the intermediate compound at 160 °C. Note that the scattering of the individual data points is due to the relatively low intensity of the (–101) peak and the reflection of the intermediate.

The temperature dependence of the reactions was investigated between 160 and 190 °C. The time until the first crystallites are observed is the induction time t_0, which depends on the reaction temperature. Increasing the temperature leads to a significant decrease of t_0. Typical for solid-state kinetics are sigmoidal curves plotting the extent of reaction $\alpha(t)$ vs. time. The curves presenting the growth of the (200) reflection of **2** at different temperatures are shown in Figure 11, and the evolution of the crystalline intermediate plotted together with the growth of the (200) reflection of **2** and the (–101) reflection of **1** at 160 °C is displayed in Figure 10.

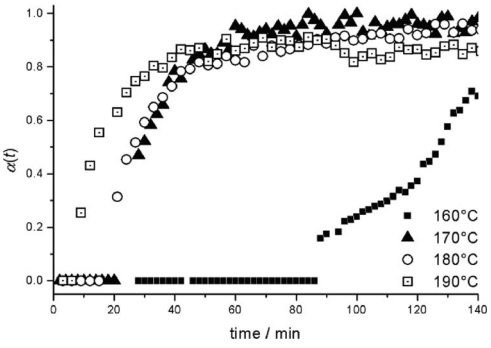

Figure 11. Temperature dependence of the crystallization of $(DBNH)_2Cu_6Sn_2S_8$ (**2**).

It is interesting to note that t_0 for the formation of **2** is reduced by roughly 60 min when the temperature is raised from 160 to 170 °C (Figure 11). For the reaction temperatures 170–190 °C, t_0 is very similar, and the product growth is very fast. In addition, the reactions at higher temperatures are finished after about 100 min.

A qualitative comparison of the reactions using Cu, Sn, S and DBN with those performed without Cu clearly demonstrates that the induction time t_0 is drastically reduced to 20 min at 160 °C (110 min with Cu) and to 4 min at 190 °C

(42 min with Cu). In the competitive crystallization it seems that the formation of **2** is preferred and the growth of **1** is inhibited.

The sizes of the coherent scattering particles of both compounds can be estimated by applying the Scherrer equation:

$$D_k = \frac{K \cdot \lambda \cdot 180/\pi}{d_{FWHM} \cdot \cos\theta}$$

where D_k is the average crystallite size, d_{FWHM} is the full width at half maximum, θ is the Bragg angle, λ is the wavelength and K is the Scherrer constant (0.89 was used). The value for d_{FWHM} of the (200) peak of **2** (θ = 4.14°) decreases from 0.22 to 0.16° during the reaction (t = 240 min) to lead to an increase of the coherent scattering domains from 36 to 49 nm. The d_{FWHM} for the (002) reflection of **1** (θ = 4.72°) is reduced from 0.2 to 0.17° to yield sizes of 39 and 46 nm for these domains, respectively.

Ex-situ experiments were performed to further explore the role of the intermediate in the formation of **1** and **2**. In treating the intermediate with DBN at 160 °C for 5 h, elemental crystalline Sn and an amorphous phase containing Cu, Sn and S are formed. Performing this reaction under similar conditions but with the addition of S produces Sn and Cu sulfides. However, in the XRD results a peak at 7.7° 2θ is observed which cannot be assigned to known Sn/Cu sulfides or the title compounds. Several experiments were conducted with the intermediate by subjecting it to different reaction conditions, but in all cases the title compounds were not formed. Two important conclusions can be drawn from this observation: (i) in accordance with the results of the in-situ EDXRD investigations, the transient crystalline compound can be regarded as a new material which is not necessary for the formation of **1** and **2**; (ii) under the real solvothermal conditions, soluble species are present which are important for the formation of **1** and **2**.

Further experiments were done to explore whether **1** can be transformed to **2**. Cu, S and DBN were added to a small amount of **1** and heated at 170 °C for 5 h. The EDX analysis yields a Cu/Sn/S ratio of 3:1:4, but the powder diffraction pattern confirms the presence of **1** and **2**.

Spectroscopy

Raman spectroscopy

In the Raman spectra, the resonances of compound **1** at 367, 336, 313 and 258 cm^{-1} are in the region typical for Sn–S resonances.[60,61] The symmetric Sn–S stretching vibration is located at 367 cm^{-1}, and symmetric Sn–$S_{bridging}$ modes appear at 336 and 313 cm^{-1}. The resonance at 258 cm^{-1} is caused by a Sn_2S_2 ring vibration. For compound **2** only two modes are observed: the band at 362 cm^{-1} is the symmetric Sn–S stretching vibration, and that at 332 cm^{-1} is the symmetric Sn–$S_{bridging}$ vibration. Surprisingly, no resonances or modes caused by Cu–S vibrations are observed.

UV/Vis spectroscopy

The optical bandgap was determined from UV/Vis diffuse reflectance spectra transformed with the Kubelka–Munk method. For **1**, E_g amounts to 2.6 eV (477 nm), in agreement with the yellow color of the material. The E_g value of 1.84 eV (674 nm) for **2** is consistent with the red color of the plates.

Thermal Stability

Compound **1** decomposes in two steps. The first thermal reaction starts at T_{onset} = 229 °C (T_{peak} = 234 °C) and is associated with a mass loss of 11.2%. The next step occurs at T_{onset} = 288 °C (T_{peak} = 310 °C) with a weight change of 21.5%. The difference between observed and calculated weight loss [–Δm_{theo} (2 DBN + 1 H_2S) = 35.3%] can be explained by a contamination (CHN) of the residue. The decomposition product is black, and SnS was identified in the powder pattern.

The thermal decomposition of compound **2** starts at T_{onset} = 218 °C (T_{peak} = 281 °C) with a related weight loss of 28.9%, which is slightly higher than the calculated value [–Δm_{theo} (DBN + H_2S) = 28.3%]. The powder obtained is black and contains a few percent of CHN. Both SnS and CuS compounds were identified in the powder pattern.

Conclusions

Under solvothermal conditions the new thiostannates, $(DBNH)_2Sn_3S_6$ (**1**) and $(DBNH)_2Cu_6Sn_2S_8$ (**2**), were obtained simultaneously as yellow needles and red plates, respectively. The quality of the crystals could be increased by using longer reaction times. The simultaneous occurrence of the mixed-valent thiostannate **1** and a Sn^{IV}-containing Cu thiostannate **2** is of special interest. Obviously, a complex redox reaction occurs over the course of the synthesis.

The Sn^{II} atom in **1** is in a trigonal pyramidal coordination environment, which is quite rare. The layered structure of **2** may be viewed as an inorganic 6^3 graphene layer constructed by the condensation of CuS_3 triangles and SnS_4 tetrahedra. Such a structural motif has never been observed in the structures of thiostannates.

Despite a large variation of several synthesis parameters, compound **2** could not be obtained as a pure phase. In-situ EDXRD experiments not only reveal that **1** and **2** start to crystallize within a narrow time window, but also highlight the occurrence of a crystalline intermediate prior to the formation of **1** and **2**. This intermediate is a new metastable compound, which is not simply transformed into the final products. The quenched metastable compound could not be transformed into either of the two stable compounds. The successful preparation of the Sn^{II}/Sn^{IV} compound demonstrates that neither the intermediate nor Cu is directly involved in the complex redox reaction. The in-situ experiments also show that crystallization of **1** is retarded in the presence of Cu species in the solution. The results of in-

situ experiments of reactions with only Sn, S, and DBN demonstrate that **2** is formed within a couple of minutes. Such information cannot be acquired using only ex-situ syntheses.

Despite the large amount of information acquired in these studies, several synthetic challenges are left open. For instance, it would be of great interest to synthesize the metastable intermediate for structural characterization. The challenge here lies in finding synthesis conditions where only this metastable compound is formed, or at least crystals of this material of appropriate quality are present. It is also necessary to synthesize a pure phase of **2**, and further explorative syntheses with different Cu and Sn compounds are underway. However, changing the starting material requires the completion of a large number of experiments in order to establish the reaction conditions for the formation of the desired compound.

Experimental Section

Syntheses

General: All chemicals were purchased (see below for purity and company) and used without further purification. Both compounds were prepared under solvothermal conditions in teflon-lined steel autoclaves (inner volume: 30 mL). The crystalline reaction products were filtered off, washed with water and ethanol and dried in vacuo.

Synthesis of $(DBNH)_2Sn_3S_6$ (1) and $(DBNH)_2Cu_6Sn_2S_8$ (2): Sn (118.7 mg, 1 mmol, 99.5%, Aldrich), Cu (63.5 mg, 1 mmol, 99.5%, Alfa Aesar) and S (105.8 mg, 3.3 mmol) were reacted in 1,5-diazabicyclo[4.3.0]non-5-ene (1.5 mL, ≥ 98.0%, Fluka) for 27 d at 140 °C, followed by cooling to 25 °C in 30 h. In the reaction products, yellow needles of **1** and red plates of **2** were found in a total yield of 30 mg (10.4%). The compounds could also be obtained with a reaction time of 5 d, but the quality of the crystals in this case, especially for **2**, was not good enough for single crystal structure determination. During the optimization of the reaction conditions, the duration was elongated from 5 up to 27 d. In all syntheses Cu and Sn sulfides were the main products. A large number of syntheses were performed to optimize the yield and the homogeneity of the products. Compound **1** could also be synthesized by the reaction of Sn (1 mmol) and S (3 mmol) in DBN (3 mL) for 20 d at 170 °C in a yield of 25 mg (11.1%). The different reaction products were manually separated, and the homogeneity of both compounds was confirmed by X-ray powder diffraction. Elemental analyses (results in %): **1**: $C_{14}H_{26}N_4Sn_3S_6$ (798.82): calcd. C 21.10, H 3.04, N 7.03; found C 21.05, H 3.21, N 7.11; **2**: $C_{14}H_{26}N_4Cu_6Sn_2S_8$ (1125.49): calcd. C 14.94, H 2.33, N 4.98; found C 14.82, H 2.46, N 4.81. The following IR absorptions were detected for the DBN molecules: **1**: $\tilde{\nu}$ = 3277 (m, –NH stretch), 3104 (m, –NH stretch), 2922 (s, $–CH_2$; m–s, –NH stretch), 1670 (m, –CC), 1567 (m–s, –NH), 1417, 1298, 1201 (m, –CN) and 1064 (m, –CN) cm^{-1}; **2**: $\tilde{\nu}$ = 2920 (s, $–CH_2$; m–s, –NH stretch), 1670 (m, –CC), 1371, 1292, 1124 (m, –CN) and 1064 (m, –CN) cm^{-1}.

Structure Determination: Intensity data were collected on a STOE IPDS-1 (Imaging Plate Diffraction System) with Mo-K_α radiation at room temperature. The structures were solved with direct methods using the program SHELXS-97,[62] and the refinements were done against F^2 with SHELXL-97.[63] Anisotropic displacement parameters were used for all non-hydrogen atoms. The H atoms of the amines were positioned with idealized geometry and refined using a riding model and a fixed isotropic displacement parameter. In **2** some disorder of the DBN is present and the structure refinement was performed using a split model. Some selected refinement results are summarized in Table 3.

CCDC-709992 (for **1**) and -709993 (for **2**) contain the supplementary crystallographic data for this paper. These data can be obtained free of charge from the Cambridge Crystallographic Data Centre via www.ccdc.cam.ac.uk/data_request/cif.

Energy Dispersive X-ray Diffraction (EDXRD): All EDXRD experiments were carried out at the HASYLAB F3 beamline at DESY, Hamburg, Germany. The beamline station receives white synchrotron radiation from a bending magnet with E_c = 16.6 keV and gives a positron beam energy of 4.5 GeV. The energy range from 6 to 60 keV exhibits a maximum at about 20 keV. A liquid nitrogen cooled solid-state germanium detector with a resolution

Table 3. Selected technical details of data collection and results of the structure refinement of the title compounds.

	$(DBNH)_2Sn_3S_6$	$(DBNH)_2Cu_6Sn_2S_8$
Crystal system	monoclinic	orthorhombic
Space group	$P2_1/n$	$Pca2_1$
a / Å	9.5822(8)	21.3017(10)
b / Å	13.1199(7)	6.6837(3)
c / Å	19.9506(16)	19.9480(13)
α / °	90	90
β / °	97.192(10)	90
γ / °	90	90
V / Å^3	2488.4(3)	2840.1(3)
Z	4	4
ρ_{calc} / g cm^{-3}	2.132	2.632
μ / mm^{-1}	3.501	6.734
Scan range	$2.65 \leq \Theta \leq 28.02°$	$2.80 \leq \Theta \leq 28.02°$
Reflections collected	21603	16982
Reflections with $F_o > 4\sigma(F_o)$	1536	2160
Independent reflections	5831 [R_{int} = 0.0589]	6810 [R_{int} = 0.0636]
Goodness-of-fit on F^2	1.006	0.985
Final R indices [$I > 2\sigma(I)$]	R_1 = 0.0387, wR_2 = 0.0874	R_1 = 0.0441, wR_2 = 0.1031
R indices (all data)	R_1 = 0.0626, wR_2 = 0.0958	R_1 = 0.0597, wR_2 = 0.1108
Residual electron density / e Å^{-3}	0.928/–0.971	1.667/–1.634
Flack x parameter		–0.02(2)

of about 1% was used. The angle of the detector was fixed at approximately 1.8° which allowed the detection of the Bragg reflections, and the observable *d*-spacing range was 3.1 to 32.3 Å given by $E = 6.199/(d\sin\theta)$. The beam was collimated to 200 × 200 mm to give the best results. More experimental details can be found in ref.[30,31] The in-situ investigations were conducted in glass tubes in special autoclaves with an internal diameter of 10 mm and a volume of 7 mL. The delay time between filling the autoclaves with the mixture of starting materials and starting the reaction was about 2 min, and the reaction temperature was reached within 1 min. Time-resolved X-ray powder patterns with acceptable counting statistics could be recorded with acquisition times between 120 and 180 s. Under stirring conditions the compounds were synthesized using Cu (30 mg, 0.47 mmol), Sn (60 mg, 0.5 mmol) and S (50 mg, 1.55 mmol) in DBN (1 mL) at temperatures ranging from 140 to 200 °C. Compound **1** was prepared using Sn (60 mg, 0.5 mmol) and S (50 mg, 1.55 mmol) in DBN (1 mL) at temperatures between 140 and 190 °C. The resulting spectra were evaluated with EDXPowd[64] and the Origin6.0 program package. Because of some problems in integrating triple peaks of the spectra series, we used the program "calf3," which was developed in close cooperation with A. Rothkirch (Hasylab, DESY). It was written to support the energy calibration of the F3 beamline and to evaluate spectra time series of in-situ EDXRD measurements. The routine is written in Interactive Data Language (IDL), ITT Visual Information Solutions, Boulder, CO, USA and runs also with IDL virtual machine. For the data evaluation of time series, an input file must be supplied that provides regions of interest for possible peak positions and (optional) regions for the background. The data are background-corrected with a polynomial function, and regions of interest are scanned for diffraction/fluorescence peaks. The peaks are fit to Gaussian functions (possible for single or even superimposed triple peaks) and integrated separately for every single spectrum. In addition, the integrals can be normalized to a reference (e.g., the integral of a fluorescence peak within a single spectrum). The coefficients and integrals thus derived are written to an output file as well as an illustration for first visual analysis. The integrals of the product reflections were normalized with the integrals of the intensity of the Sn-*Kα* fluorescence peak.

X-ray Powder Diffraction: X-ray powder diffraction patterns were recorded in transmission mode with a STOE Stadi-P diffractometer equipped with an imaging-plate position-sensitive detector (IP-PSD) and a Ge monochromator using Cu-$K_\alpha 1$ (λ = 1.54056 Å) radiation.

Thermal Investigations: DTA-TG experiments were carried out using a Netzsch STA 429 DTA-TG device. The samples were heated up to 500 °C at 4 K min^{-1} under a flow of argon (75 mL min^{-1}) in Al_2O_3 crucibles. The TG data were corrected for buoyancy and current effects.

Scanning Electron Microscopy (SEM)/Energy Dispersive X-ray Fluorescence (EDX): A Philips ESEM XL30 equipped with an EDAX EDX system was used to determine the compositions.

Raman Spectroscopy: The data for the Raman spectra were collected in the 100 to 500 cm^{-1} region with a Bruker IFS 66 Fourier Transform Raman spectrometer (wavelength: 541.5 nm).

UV/Vis Spectroscopy: Investigations were done at room temperature using a UV/Vis/NIR two-channel Cary 5 spectrometer from Varian Techtron Pty., Darmstadt. The absorption data were calculated with the Kubelka-Munk approach for diffuse reflectance data. $BaSO_4$ powder was used as reference material.

Elemental Analysis: CHNS analyses were done using a EURO EA Elemental Analyzer, fabricated by EURO VECTOR Instruments and Software.

Acknowledgments

We thank the Hasylab, DESY, Hamburg, Germany, for the measurement times at the F3 beamline. Thanks to Beatrix Seidlhofer and Elena Antonova (University of Kiel) for joining our measurements and thanks to André Rothkirch (Hasylab, DESY, Hamburg) for his help.

[1] M. Behrens, C. Näther, W. Bensch, *Z. Anorg. Allg. Chem.* **2002**, *628*, 2160.
[2] C. Näther, S. Scherb, W. Bensch, *Acta Crystallogr., Sect. E* **2003**, *59*, m280–m282.
[3] A. Puls, C. Näther, W. Bensch, *Acta Crystallogr., Sect. E* **2005**, *61*, m868–m870.
[4] J. B. Parise, Y. Ko, J. Rijssenbeek, D. M. Nellis, K. Tan, S. Koch, *J. Chem. Soc., Chem. Commun.* **1994**, 527.
[5] T. Jiang, A. Lough, G. A. Ozin, *Adv. Mater.* **1998**, *10*, 42–46.
[6] T. Jiang, A. Lough, G. A. Ozin, R. L. Bedard, R. Broach, *J. Mater. Chem.* **1998**, *8*, 721–732.
[7] S. Dehnen, C. Zimmermann, *Z. Anorg. Allg. Chem.* **2002**, *628*, 2436–2439.
[8] R. W. J. Scott, M. J. MacLachlan, G. A. Ozin, *Curr. Opinions Solid State Mater. Science* **1999**, *4*, 113–121.
[9] T. Jiang, G. A. Ozin, *J. Mater. Chem.* **1997**, *7*, 2213–2222.
[10] R. J. Francis, S. J. Price, J. S. O. Evans, S. O'Brien, D. O'Hare, S. M. Clark, *Chem. Mater.* **1996**, *8*, 2102–2108.
[11] Y. An, M. Ji, M. Baiyin, X. Liu, C. Jia, D. Wang, *Inorg. Chem.* **2003**, *42*, 4248–4249.
[12] M. Behrens, S. Scherb, C. Näther, W. Bensch, *Z. Anorg. Allg. Chem.* **2003**, *629*, 1367–1373.
[13] N. Pienack, W. Bensch, *Z. Anorg. Allg. Chem.* **2006**, *632*, 1733–1736.
[14] N. Pienack, C. Näther, W. Bensch, *Solid State Sci.* **2007**, *9*, 100–107.
[15] D. X. Jia, J. Dai, Q. Y. Zhu, Y. Zhang, X. M. Gu, *Polyhedron* **2004**, *23*, 937–942.
[16] M. Antonietti, G. A. Ozin, *Chem. Eur. J.* **2004**, *10*, 28–41.
[17] M. Cruz, J. Morales, J. P. Espinos, J. Sanz, *J. Solid State Chem.* **2003**, *175*, 359–365.
[18] K. O. Klepp, F. Fabian, *Z. Naturforsch., Teil B* **1992**, *47*, 406–410.
[19] K. O. Klepp, F. Fabian, *European Crystallographic Meeting* **1994**, *15*, 626–626.
[20] S. Chitsaz, B. Neumüller, K. Dehnicke, *Z. Anorg. Allg. Chem.* **2000**, *626*, 318–815.
[21] J. F. Eichler, O. Just, W. S. Rees, *Inorg. Chem.* **2006**, *45*, 6706–6712.
[22] C. Adenis, J. Olivier-Fourcade, J. C. Jumas, E. Philippot, *Rev. Chim. Min.* **1986**, *23*, 735–745.
[23] C. Adenia, J. Olivier-Fourcade, J. C. Jumas, E. Philippot, *Eur. J. Solid State Inorg. Chem.* **1988**, *25*, 413–423.
[24] J. C. Jumas, J. Olivier-Fourcade, E. Philippot, M. Maurin, *Rev. Chim. Min.* **1979**, *16*, 48–59.
[25] S. Jobic, P. le Boterf, R. Brec, G. Ouvrard, *J. Alloys Compd.* **1994**, *205*, 139–145.
[26] R. Francis, D. O'Hare, *J. Chem. Soc., Dalton Trans.* **1998**, 3133.
[27] W. Bensch, C. Näther, R. Stähler, *Chem. Commun.* **2001**, 477–478.
[28] R. Stähler, B. D. Mosel, H. Eckert, W. Bensch, *Angew. Chem. Int. Ed.* **2002**, *41*, 4487–4489.
[29] R. Kiebach, F. Studt, C. Näther, W. Bensch, *Eur. J. Inorg. Chem.* **2004**, 2553–2556.
[30] L. Engelke, M. Schaefer, M. Schur, W. Bensch, *Chem. Mater.* **2001**, *13*, 1383–1390.

[31] L. Engelke, M. Schaefer, F. Porsch, W. Bensch, *Eur. J. Inorg. Chem.* **2003**, 506–513.
[32] R. Kiebach, M. Schaefer, F. Porsch, W. Bensch, *Z. Anorg. Allg. Chem.* **2004**, *631*, 369–374.
[33] R. Kiebach, N. Pienack, M. E. Ordolff, F. Studt, W. Bensch, *Chem. Mater.* **2006**, *18*, 1196–1205.
[34] A. Michailovski, J.-D. Grunwaldt, A. Baiker, R. Kiebach, W. Bensch, G. R. Patzke, *Angew. Chem.* **2005**, *117*, 5787–5792; *Angew. Chem. Int. Ed.* **2005**, *44*, 5643–5647.
[35] A. Michailovski, R. Kiebach, W. Bensch, J.-D. Grunwaldt, A. Baiker, S. Komarneni, G. R. Patzke, *Chem. Mater.* **2007**, *19*, 185–197.
[36] R. Kiebach, N. Pienack, W. Bensch, J.-D. Grunwaldt, A. Michailovski, A. Baiker, T. Fox, Y. Zhou, G. R. Patzke, *Chem. Mater.* **2008**, *20*, 3022–3033.
[37] R. I. Walton, T. Loiseau, D. O'Hare, G. Férey, *Chem. Mater.* **1999**, *11*, 3201–3209.
[38] K. Tan, Y. Ko, J. B. Parise, *Acta Crystallogr., Sect. C* **1995**, *51*, 398.
[39] T. Jiang, A. J. Lough, G. A. Ozin, D. Young, R. L. Bedard, *Chem. Mater.* **1995**, *7*, 245–248.
[40] O. Slupecki, I. D. Brown, *Acta Crystallogr., Sect. B* **1982**, *38*, 1078–1079.
[41] R. Kniep, D. Mootz, U. Severin, H. Wunderlich, *Acta Crystallogr., Sect. B* **1982**, *38*, 2022.
[42] J. J. Vittal, P. A. W. Dean, *Acta Crystallogr., Sect. C: Cryst. Struct. Commun.* **1996**, *52*, 1180.
[43] P. A. W. Dean, J. J. Vittal, N. C. Payne, *Can. J. Chem.* **1985**, *63*, 394.
[44] G. Barone, T. G. Hibbert, M. F. Mahon, K. C. Molloy, I. P. Parkin, L. S. Price, I. Silaghi-Dumitrescu, *J. Chem. Soc., Dalton Trans.* **2001**, 3435.
[45] T. Jiang, A. Lough, G. A. Ozin, R. L. Bedard, *J. Mater. Chem.* **1998**, *8*, 733–741.
[46] W. S. Sheldrick, B. Schaaf, *Z. Anorg. Allg. Chem.* **1994**, *620*, 1041–1045.
[47] T. Jiang, G. A. Ozin, *J. Mater. Chem.* **1998**, *8*, 1099–1108.
[48] T. Jiang, G. A. Ozin, R. L. Bedard, *J. Mater. Chem.* **1998**, *8*, 1641–1648.
[49] X. Chen, H. Wada, A. Sato, M. Mieno, *J. Solid State Chem.* **1998**, *139*, 144–151.
[50] X. Chen, H. Wada, A. Sato, *Mater. Res. Bull.* **1999**, *34*, 239.
[51] V. Spetzler, H. Rijnberk, C. Näther, W. Bensch, *Z. Anorg. Allg. Chem.* **2004**, *630*, 142–148.
[52] V. Spetzler, C. Näther, W. Bensch, *Inorg. Chem.* **2005**, *44*, 5805–5812.
[53] M. Jansen, *Angew. Chem.* **1987**, *99*, 1136–49; *Angew. Chem. Int. Ed. Engl.* **1987**, *26*, 1098–1110.
[54] R. Stähler, C. Näther, W. Bensch, *J. Solid State Chem.* **2003**, *174*, 264–275.
[55] M. J. Avrami, *Chem. Phys.* **1939**, *7*, 1103–1112.
[56] M. J. Avrami, *Chem. Phys.* **1940**, *8*, 212–224.
[57] M. J. Avrami, *Chem. Phys.* **1941**, *9*, 177–184.
[58] J. H. Sharp, G. W. Brindley, B. N. Narahari Achar, *J. Am. Ceram. Soc.* **1966**, *47*, 379–382.
[59] J. D. Hancock, J. H. Sharp, *J. Am. Ceram. Soc.* **1972**, *55*, 74–76.
[60] B. Krebs, W. Schiwy, *Z. Anorg. Allg. Chem.* **1973**, *398*, 63–71.
[61] B. Krebs, S. Pohl, W. Schiwy, *Angew. Chem.* **1970**, *82*, 884–885; *Angew. Chem. Int. Ed. Engl.* **1970**, *9*, 897–898.
[62] G. M. Sheldrick, *SHELXS 97, Program for the Solution of Crystal Structures*, University of Göttingen, Germany, **1997**.
[63] G. M. Sheldrick, *SHELXL 97, Program for the Refinement of Crystal Structures*, University of Göttingen, Germany, **1997**.
[64] F. Porsch, *EDXPowd Version 3.155*, RTI GmbH, Paderborn, Germany, **2004**.

Received: November 5, 2008
Published Online: February 5, 2009

